Chemical Engineering Journal 144 (2008) 431–441

Contents lists available at ScienceDirect

Chemical Engineering Journal

journal homepage: www.elsevier.com/locate/cej

Separation of lead ions from wastewater using electrodialysis: Comparing mathematical and neural network modeling

Mohtada Sadrzadeh[a], Toraj Mohammadi[a,*], Javad Ivakpour[b], Norollah Kasiri[b]

[a] *Research Lab for Separation Processes, Department of Chemical Engineering, Iran University of Science and Technology (IUST), Narmak,Tehran, Iran*

[b] *Computer Aided Process Engineering (CAPE) Lab, Department of Chemical Engineering, Iran University of Science and Technology (IUST),Narmak, Tehran, Iran*

ARTICLE INFO

Article history:
Received 25 September 2007
Received in revised form 15 February 2008
Accepted 20 February 2008

Keywords:
Electrodialysis
Neural network
Mathematical modeling
Wastewater treatment
Metal ions

ABSTRACT

This paper presents experimental data, an artificial neural network (ANN) model and a mathematical model (MM) for a laboratory scale electrodialysis (ED) cell. The aim was to predict separation percent (SP) of Pb^{2+} ions as a function of concentration, temperature, flow rate and voltage. The MM started from a differential equation of steady state mass balance. Neglecting resistances of ion exchange membranes compared with resistances of bulk solutions in dilute and concentrate compartments and deriving a relation for solution resistance as a function of operating parameters, the final one-parameter model was obtained. The applied ANN was a multilayer perceptron (MLP) network with two hidden layers. The fast Levenberg–Marquardt (LM) optimization technique was employed for training the ANN. MM and ANN were able to predict the performance of ED desalination with correlation coefficients of 0.97 and 0.99, respectively. Comparing MM and ANN model results, it was found that ANN model is more capable than MM to predict nonlinear behavior of ED process. However, MM is more efficient at higher feed flow rates and lower voltages, temperatures and feed concentrations. ANN is found out to be an efficient tool to model the complicated ion transfer mechanism in an electrical field.

1. Introduction

Many industrial wastewaters produced by metal plating, metal finishing, mining, automotive, aerospace, battery and general chemical plants, often contain high concentration of heavy metals [1]. Lead is a highly toxic heavy metal. It impairs hemoglobin synthesis, particularly in children, and may cause neurological disorders. Lead is found in water and air. Wastes that include lead are found in paints, pipes, batteries and in some petrol types [2].

Processes developed to remove heavy metals such as lead from wastewaters include chemical precipitation [3], coagulation, complexing, solvent extraction [4–6], ion exchange [7,8], biosorption [9–13], electro-membrane processes [14–16] and adsorption on solid surfaces. These processes have some inherent shortcomings such as requiring a large area of land, a sludge dewatering facility, skillful operators, multiple basin configurations and high capital and regeneration costs of activated carbon and ion-exchange resins [17].

Membranes can also be used to obtain effluents without metallic contaminants. The main disadvantage of membrane processes for treatment of effluents with heavy metals is ionic size of dissolved metallic salts. These ions, as hydrated ions or as low molecular weight complexes, pass easily through all membranes with the exception of reverse osmosis membranes. However, reverse osmosis membranes are not selective, because interesting metallic ions are retained together with alkaline and alkaline–earth ions [1].

ED is an electrochemical process for separation of ions across charged membranes from one solution to another under the influence of an electrical potential difference used as a driving force. This process has been widely used for production of drinking and process water from brackish water and seawater, treatment of industrial effluents, recovery of useful materials from effluents and salt production. The basic principles and applications of ED were reviewed in the literature [18–20].

ANN utilizes interconnected mathematical nodes or neurons to form a network that can model complex functional relationships [21]. Its development started in the 1940s to help cognitive scientists to understand the complexity of the nervous system. It has been evolved steadily and was adopted in many areas of science. Basically, ANNs are numerical structures inspired by the learning process in the human brain. They are constructed and used as alternative mathematical tools to solve a diversity of problems in the fields of system identification, forecasting, pattern recognition, classification, process control and many others [22].

* Corresponding author. Tel.: +98 21 77240496; fax: +98 21 77240495.
E-mail address: torajmohammadi@iust.ac.ir (T. Mohammadi).

1385-8947/$ – see front matter © 2008 Elsevier B.V. All rights reserved.
doi:10.1016/j.cej.2008.02.023

Nomenclature

a	ion hydrodynamic radius, input data in ANN
A_m	effective area of ion exchange membrane (m^2)
b	bias or nodes internal threshold
C	concentration ($kmol\,m^{-3}$)
D	diffusivity ($m^2\,s^{-1}$)
e	electronic charge (C)
E	electrical potential (V)
f	function
F	Faraday constant ($C\,kmol^{-1}$)
h	thickness of dilute compartment (m)
i	current density ($A\,m^{-2}$)
I	current intensity (A)
J	molar flux ($kmol\,m^{-2}\,s^{-1}$)
k	mass transfer constant ($m\,s^{-1}$)
K	Kohlrausch coefficient ($S\,m^2\,kmol^{-1}\,M^{-0.5}$)
l	flow length in channel (m)
MSE	mean squared error
N	number of cell pairs, number of validation and training data
q	constant
Q	flow rate ($m^3\,s^{-1}$)
R	resistance (Ω)
SP	separation percent (%)
T	temperature (K)
u	flow velocity ($m\,s^{-1}$)
w	width of ED cell (m), weight factor in ANN
x	coordinate (m)
x'	constant ($C^2\,s\,kmol^{-1}\,kg^{-1}$)
y'	constant ($S\,m^2\,kmol^{-1}\,M^{-0.5}$)
z	valence
z'	constant ($M^{-0.5}$)

Greek letters

Λ_M	molar conductivity ($S\,m^2\,kmol^{-1}$)
Λ_M^o	limiting molar conductivity ($S\,m^2\,kmol^{-1}$)
α	constant ($m^{4/3}\,s^{2/3}\,kg^{2/3}\,A\,kmol^{-1}\,K^{-2/3}$)
β	constant ($kmol\,K^{2/3}\,s^{1/3}\,m^{-7/3}\,kg^{-2/3}\,A^{-1}$)
ε	electric permittivity ($C^2\,J^{-1}\,m^{-1}$)
ε_0	permittivity in free space ($C^2\,J^{-1}\,m^{-1}$)
ε_r	relative permittivity
γ'	constant ($s\,m^{-1}$)
γ	constant ($s\,m^{-1}$)
η	current efficiency
μ	viscosity ($kg\,m^{-1}\,s^{-1}$)
ρ	density ($kg\,m^{-3}$)
κ	conductivity ($S\,m^{-1}$)
λ	molar conductivity of ions ($S\,m^2\,kmol^{-1}$)
ν	stochiometric constant
υ	mobility of ions ($m^2\,s^{-1}\,V^{-1}$)
ω, σ and δ	constant
ψ	Debye–Huckel–Onsager coefficient ($M^{-0.5}$)
ζ	Debye–Huckel–Onsager coefficient ($S\,m^2\,kmol^{-1}\,M^{-0.5}$)
$\Re$	universal gas constant ($J\,kmol^{-1}\,K^{-1}$)

Subscripts

cal	calculated
d	dilute compartment
exp	experimental
m	membrane
M	molar
±	cation or anion
0	initial condition

In recent years, ANNs have been used as a powerful modeling tool in various membrane processes such as membrane filtration (FT) [23,24], microfiltration (MF) [25–29], ultrafiltration (UF) [30–45], nanofiltration (NF) [46–49], reverse osmosis (RO) [50–55], gas separation (GS) [56,57], membrane bioreactors (MBRs) [58,59] and fuel cells (FC) [60,61]. Key features of previous studies are summarized in Table 1. According to this table, it can be concluded that:

1. RO and MF were the earliest membrane processes modeled and simulated by ANN.
2. Researchers have recently focused on modeling of GS and MBRs using ANN. However, ongoing works have also been accomplished on traditional membrane processes, lately.
3. ANN modeling of UF was most frequently observed in the literature.
4. The most popular form of ANN in use was feed forward neural network (FFNN) modeling.
5. Of FFNN, MLP and radial basis function (RBF) were by far the most widely used in membrane processes.
6. Almost all the researchers applied back propagation (BP) training method for their ANN.
7. RO and NF water desalination processes were modeled by ANN previously.
8. No record for modeling of ED desalination by ANN was found in the literature.

The objective of this paper is to compare the SP values of lead ions predicted by MLP neural network model with those of MM and experimental data. ANN model was found out to be more capable to predict the nonlinear behavior of an ED process than MM.

2. ANN theory

ANN is an information processing system that is inspired by the way such as biological nervous systems e.g. brain. The objective of a neural network is to compute output values from input values by some internal calculations [31]. The basic component of a neural network is the neuron, also called "node". Fig. 1 illustrates a single node of a neural network.

Inputs are represented by a_1, a_2 and a_n, and the output by O_j. There can be many input signals to a node. The node manipulates these inputs to give a single output signal [62].

The values w_{1j}, w_{2j}, and w_{nj}, are weight factors associated with the inputs to the node. Weights are adaptive coefficients within the network that determine the intensity of the input signal. Every input $(a_1, a_2, \ldots, a_n)$ is multiplied by its corresponding weight factor $(w_{1j}, w_{2j}, \ldots, w_{nj})$, and the node uses summation of these weighted inputs $(w_{1j}a_1, w_{2j}a_2, \ldots, w_{nj}a_n)$ to estimate an output signal using a transfer function.

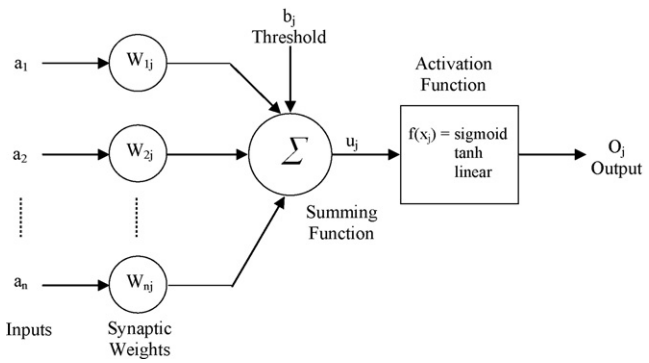

Fig. 1. Single node anatomy.

Table 1
Summary of researchers' studies in modeling of membrane processes by ANN

Reference	Year	Membrane process	ANN type	Training method	ANN application
Dornier et al. [25]	1995	MF	FFNN[a]–MLP[b]	SL[c]–BP[d]	Modeling of crossflow MF
Niemi et al. [50]	1995	RO	FFNN–MLP	SL–BP	Simulation of RO membrane separation
Al-shayji and Liu [53,54]	1997, 2002	RO	FFNN–MLP	SL–BP	Modeling and optimization of large-scale commercial water desalination plants
Bowen et al. [32,33,36]	1998, 2001	UF	FFNN–MLP	SL–BP	Prediction of the rate of crossflow membrane UF of colloids
Delgrange et al. [30,31]	1998–2002	UF	FFNN–MLP	SL–BP–QNLA[e]	Modeling of UF fouling, prediction of UF transmembrane pressure in drinking water production
Hamachi et al. [27]	1999	MF	RN[f]	USL[g]	Modeling of crossflow MF of bentonite suspension
Teodosiu et al. [34]	2000	UF	FFNN–MLP	SL–BP	Predicting the time dependence of flux evolution in UF
Bowen et al.	2002	NF	FFNN–MLP	CGM[h]–SCG[i]	Predicting salt rejections at NF
Jafar and Zilouchian [55]	2001	RO	FFNN–MLP and RBF[j]	SL–BP	Modeling of an RO water desalination
Cabassud et al. [38]	2002	UF	RN	USL	Predictive control algorithm to improve the productivity of an UF
Bhattacharjee and Singh [37]	2002	UF	FFNN–MLP	SL–BP	Modeling of a continuous stirred UF process
Razavi et al. [40,41]	2003	UF	FFNN–MLP	SL–BP	Prediction of milk UF performance
Shetty et al. [47]	2003	NF	FFNN–MLP	SL–BP–LMT[k]	Prediction of contaminant removal and membrane fouling during municipal drinking water NF
Lee et al. [60]	2004	FC	FFNN–MLP	SL–BP	Modeling of polymer electrolyte membrane FC performance
Aydiner et al. [28]	2005	MF	FFNN–MLP	SL–BP	Modeling of flux decline in crossflow MF
Chellam [29]	2005	MF	FFNN–MLP	SL–BP–LMT	Modeling of transient crossflow MF of polydispersed suspensions
Zhao et al. [51]	2005	RO and NF	FFNN–MLP and NRBF[l]	SL–BP	Predicting RO/NF water quality
Abbas and Al-Bastaki [52]	2005	RO	FFNN–MLP	SL–BP–LMT	Modeling of an RO water desalination
Rai et al. [43]	2005	UF	FFNN–MLP	SL–BP	Modeling batch UF of synthetic fruit juice and mosambi juice
Geissler et al. [58]	2005	MBR	SRN[m] (EN[n])	SL–BP	Modeling of capillary modules in MBR
Ou et al. [61]	2005	FC	FFNN–MLP and RBF	SL–BP	Modeling of proton exchange membranes
Chen and Kim [24]	2006	FT	FFNN–MLP and RBF	SL–BP–LMT	Prediction of permeate flux decline in crossflow membrane FT
Cinar et al. [59]	2006	MBR	CFNN[o]–MLP	SL–BP	Modeling of submerged MBR treating cheese whey wastewater
Curcio et al. [45]	2006	UF	FFNN–MLP	SL–BP	Reduction and control of flux decline in cross-flow UF
Wang et al. [57]	2006	GS	FFNN–RBF	SL–BP	Modeling of hydrogen recovery from refinery gases
Sahoo and Ray [23]	2006	FT	FFNN–RBF	SL–BP–LMT	Prediction of flux decline in crossflow membranes
Shahsavand et al. [56]	2007	GS	FFNN–MLP and RBF	SL–BP	Modeling the separation of CO_2 from CH_4 using hollow fiber module
Al-Zoubi et al. [49]	2007	NF	FFNN–MLP	SL–BP	Modeling the rejection of sulphate and potassium salts by NF

[a] Feed forward neural network.
[b] Multilayer perceptron.
[c] Supervised learning.
[d] Back propagation.
[e] Quasi newton learning algorithm.
[f] Recurrent network.
[g] Unsupervised learning.
[h] Conjugate gradient method.
[i] Scaled conjugate gradient.
[j] Radial basis function.
[k] Levenberg–Marquardt technique.
[l] Normalized radial basis function.
[m] Simple recurrent network.
[n] Elman network.
[o] Cascade forward neural network.

The other input to the node, b_j, is the node's internal threshold, also called bias. This is a randomly chosen value that governs the node's net input through the following equation:

$$u_i = \sum_{i=1}^{n} (w_{ij} a_i) - b_j \quad (1)$$

Node's output is determined using a mathematical operation on the node's net input. This operation is called a transfer function. The transfer function can transform the node's net input in a linear or nonlinear manner. Three types of commonly used transfer functions are as follows:

- Sigmoid transfer function

$$f(x) = \frac{1}{1 + e^{-x}}, \quad 0 \le f(x) \le 1 \quad (2)$$

- Hyperbolic tangent transfer function

$$f(x) = \tanh(x) = \frac{e^{x} - e^{-x}}{e^{x} + e^{-x}}, \quad -1 \le f(x) \le 1 \quad (3)$$

- Linear transfer function

$$f(x) = x, \quad -\infty \le f(x) \le +\infty \quad (4)$$

The neuron's output, O_j, is found by performing one of these functions on the neuron's net input, u_j. Neural networks are made of several neurons that perform in parallel or in sequence.

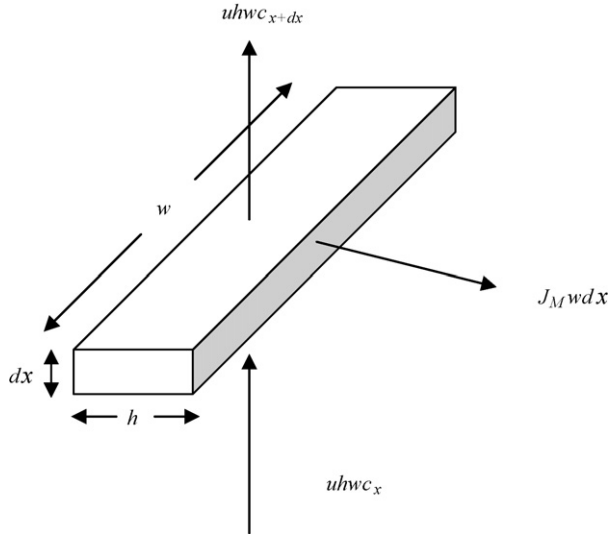

Fig. 2. Differential element of the dilute compartment.

The weight factors and thresholds are adjusted in training process. Training is the process by which the weights are adjusted systematically so that the network can predict the correct outputs for a given set of inputs. There are many different types of training algorithms. One of the most common classes of training algorithms for FFNNs is called BP [62,63]. Mathematical aspects of all training algorithms are comprehensively described in the literature [64–67].

3. Mathematical modeling

A differential element of the dilute compartment is illustrated in Fig. 2. The steady state mass balance of lead ions in the compartment is as follows:

$$uhwC_x - uhwC_{x+\mathrm{d}x} = J_\mathrm{M} w\,\mathrm{d}x \tag{5}$$

Also, the molar flux through the dilute compartment in term of current density is as follows:

$$J_\mathrm{M} = \eta\frac{i}{F} = \frac{\eta}{F}\frac{\mathrm{d}I}{\mathrm{d}A_\mathrm{m}} \tag{6}$$

where $A_\mathrm{m} = lw$, l, h and w are channel dimensions, η is current efficiency, F is Faraday constant and i is current density. Assuming constant concentration in the cell compartment ($\mathrm{d}I/\mathrm{d}A_\mathrm{m} = I/A_\mathrm{m}$), the following differential equation is obtained [68]:

$$uh\,\mathrm{d}c = -\frac{I}{A_\mathrm{m}}\frac{\eta}{F}\,\mathrm{d}x \tag{7}$$

In order to be able to use integrate form of this equation with operational variables, η needs to be verified. At any point, molar flux can be written as follows:

$$J_\mathrm{M} = k(C_\mathrm{bulk} - C_i) = k\Delta C \tag{8}$$

where C_bulk and C_i are concentrations at the bulk of dilute stream and at the membrane surface, respectively. Due to very small distance between two membranes, ΔC can be assumed to be constant along the membrane surface [68]. Hence, Eqs. (6) and (8) can be combined as follows:

$$\eta = \frac{\Delta cFA_\mathrm{m}}{I}k = \gamma' k \tag{9}$$

According to the literature, k is calculated as follows [69]:

$$k = 3.30D^{2/3}\left(\frac{Q_\mathrm{d}}{hA_\mathrm{d}l}\right)^{1/3} \tag{10}$$

In ED, the basic relations between current (I), effective electrical motive force (E) and system resistance (R) can be described by ohm's law:

$$I = \frac{E}{NR} \tag{11}$$

where N is the number of cells which is 1 in this study. Neglecting membranes resistances, solution resistance can be expressed as a function of concentration and temperature ($f(c,T)$). Table 2 shows how electrochemistry rules were applied sequentially to find this functionality [70]. Using equations in this table, the following equation can be derived:

$$R = \frac{h}{CA(x' - y'C^{0.5} - x'z'C^{0.5})} \tag{12}$$

where

$$x' = \frac{eFz^2}{6\pi\mu}\left(\frac{1}{a_+} + \frac{1}{a_-}\right), \qquad y' = \frac{3.30}{\mu(\varepsilon_\mathrm{r}T)^{0.5}} \quad \text{and} \quad z' = \frac{3281587}{(\varepsilon_\mathrm{r}T)^{1.5}}.$$

Combination of Eqs. (7)–(12) and integrating both sides using the following boundary condition result in an expression for the model parameter (γ):

At $x = 0$, $\quad C = C_0$

$$\gamma = -\frac{Q_\mathrm{d}^{2/3}}{ET^{2/3}}\frac{h^{5/3}}{(lw)^{2/3}}\left(\frac{6\pi a}{e\Re}\right)^{2/3}(F\mu)^{5/3}\int_{C_0}^{C} f(C,T)\,\mathrm{d}c \tag{13}$$

Table 2
Electrochemistry rules to find the functionality of electrolyte resistance (R)

(1) Electrolyte resistance	$R = \frac{h}{\kappa A}$	(2) Electrolyte conductivity	$\kappa = \Lambda_\mathrm{M} c$
(3) Molar conductivity	$\Lambda_\mathrm{M} = \Lambda_\mathrm{M}^\mathrm{o} - Kc^{0.5}$	(4) Limiting molar conductivity[a]	$\Lambda_\mathrm{M}^\mathrm{o} = \nu_+\lambda_+ + \nu_-\lambda_-$
(5) Ion molar conductivity	$\lambda_\pm = \frac{z_\pm F D_\pm}{\Re T}$	(6) Diffusion coefficient	$D_\pm = \frac{\upsilon_\pm \Re T}{z_\pm F}$
(7) Ion mobility[b]	$\upsilon_\pm = \frac{z_\pm e}{6\pi\mu a_\pm}$	(8) Kohlrausch coefficient	$K = \zeta + \psi\Lambda_\mathrm{m}^\mathrm{o}$
(9) Debye–Huckel–Onsager coefficient	$\zeta = \frac{z^2 \mathrm{e}\mathrm{F}^2}{3\pi\mu}\left(\frac{2}{\varepsilon\Re T}\right)^{0.5}$	(10) Debye–Huckel–Onsager coefficient	$\psi = \frac{qz^3\mathrm{e}\mathrm{F}^2}{24\pi\varepsilon\Re T}\left(\frac{2}{\varepsilon\Re T}\right)^{0.5}$
(11) Electric permittivity[c]	$\varepsilon = \varepsilon_\mathrm{r}\varepsilon_0$	(12) Relative permittivity	$\varepsilon_\mathrm{r} = 185.765 - 0.35963T$
(13) Constant[d]	$q = \frac{2\omega z_+ z_-(\lambda_+ + \lambda_-)}{(z_+ + z_-)(z_+\lambda_- + z_-\lambda_+)}$	(14) Constant[e]	$\omega = \frac{z_+ z_-(\lambda_+ + \lambda_-)}{(z_+ + z_-)(z_+\lambda_+ + z_-\lambda_-)}$

[a] Molar conductivity is the limit of zero concentration of an electrolyte. ν_+ and ν_- are the numbers of cations and anions per an electrolyte molecule (e.g. $\nu_+ = \nu_- = 1$ for $PbSO_4$). z_+ and z_- are cation and anion valances. For n–n electrolytes such as $PbSO_4$ $z_+ = z_- = z$.
[b] a in this equation is the ion hydrodynamic radius.
[c] ε_0 is the vacuum permittivity (8.854×10^{-12} C^2 J^{-1} m^{-1}).
[d] For 1–1, 2–2 and n–n electrolytes $\omega = 0.5$.
[e] $q = 0.586$ and 2.343 for 1–1 electrolyte and 2–2 electrolyte, respectively.

Using a simple change of variable, Eq. (13) can be written as a function of SP.

$$\gamma = \alpha \times \beta \tag{14}$$

where

$$\alpha = -\frac{Q_d^{2/3}\mu^{5/3}}{C_0 E T^{2/3}} \ln\left[\frac{(\delta+\sigma)\sqrt{1-SP}}{\delta+\sigma\sqrt{1-SP}}\right] \tag{15}$$

and

$$\beta = 75\frac{h^{5/3}}{(lw)^{2/3}}\left(\frac{6\pi a}{e\Re}\right)^{2/3} F^{5/3} \tag{16}$$

In Eq. (15), $\sigma = -\sqrt{C_0/T}(0.38 + 125/T)$ and $\delta = 0.026$. SP is also defined as:

$$SP = \frac{C_0 - C}{C_0} \times 100 \tag{17}$$

where C_0 and C are feed and dilute concentrations, respectively. The following equation was fitted for α as a function of operating parameters using experimental data:

$$\alpha = \frac{1}{-1.5\times10^6/E + 1.15\times10^7 C_0^{155/T}/E^{0.001} + 3\times10^{17}Q_d^{2.5}} \tag{18}$$

With the aid of Eqs. (14)–(18) and using MATLAB programming software, the model gives SP for various temperatures, feed concentrations, flow rates and voltages. Detailed description of the developed model was presented elsewhere [70,71].

4. Materials & method

4.1. Materials

An analytical grade salt (99.9% lead nitrate supplied by Merck) and deionized water were used in all experiments to produce solutions with wastewater qualities. The purpose of these experiments was to study the effects of voltage, flow rate, temperature and feed concentration on the ED cell performance.

4.2. Cell and membranes

The ED cell was packed with a pair of cation and anion exchange membranes (CEM and AEM) and a pair of platinum electrodes (anode and cathode). Both electrodes were made of pure platinum. Area of each electrode was 4.2 mm × 4.2 mm. Thickness of dilution cell (center) is 4 mm and thickness of each concentrate cell (left and right) was 3 mm. Schematic view of the applied ED cell is presented in Fig. 3. Lead nitrate solution is introduced into the three compartments. When a DC potential is applied between two electrodes, positively charged lead ions move toward the cathode, pass through the negatively charged CEM and are retained by the positively charged AEM. On the other hand, nitrate ions move toward the anode, pass through the AEM and are retained by the CEM. At the end, ion concentration increases in the side compartments with a simultaneous decrease of ion concentration in the middle compartments.

AR204SXR412 and CR67, MK111 anion and cation exchange membranes supplied by Arak petrochemical complex and made by Ionics incorporated were used in all experiments. Effective area of each membrane was 6 mm × 6.5 mm. IECs of anion and cation exchange membranes were 2.8 and 2.4 meq/g dry membrane, respectively.

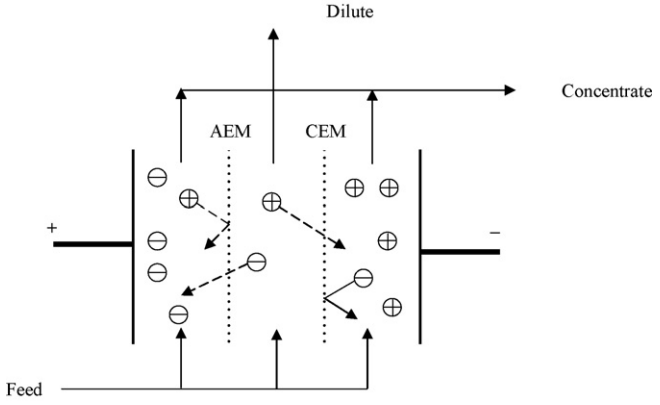

Fig. 3. Schematic view of an ED cell.

4.3. ED setup

ED setup consists of a feed tank (TK-01) where wastewater is stored, two pumps (P-01 and P-02), a rectifier (DC-01) and two globe valves (GB-01 and GB-02) to control feed flow rate in three compartments of a self designed ED cell. A simplified diagram of the setup is shown in Fig. 4.

4.4. Experimental design

Many parameters affect performance of the ED cell. According to our previous studies [2,20,68,72], four parameters were selected. It is believed that they have the greatest effect on SP: feed concentration, dilute solution flow rate, voltage and feed temperature. Four factors with their levels were studied based on the full factorial design:

- Temperature (T): 25, 40 and 60 °C.
- Concentration (C): 100, 500 and 1000 ppm.
- Flow rate (F): 0.07, 0.7 and 1.2 mL/s.
- Voltage (V): 10, 20 and 30 V.

Each experiment was lasted for about 15 min to reach steady state condition. Three samples were taken every 5 min and the average value was reported.

4.5. Analytical method

Concentration of cations (Pb^{2+}) only in the dilute compartment was measured at various operating conditions. In all experiments, atomic absorption (Shimadzu, AA-670) was used to measure the amount of lead ions in water.

4.6. ANN modeling of ED

ANN input parameters were carefully selected to only include physically meaningful and easily to measurable membrane operational and feed water quality variables as cell voltage and feed flow rate, temperature and concentration. Totally 81 experimental

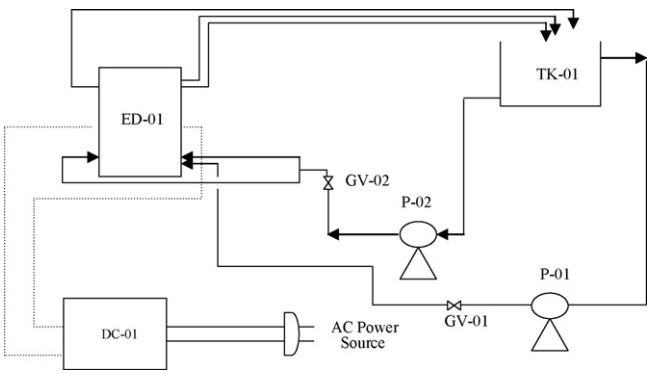

Fig. 4. A simplified diagram of the ED cell.

data are collected and used for ANN modeling of ED for training/validation/testing subsets.

In this work, feed forward multilayer neural network with two hidden layers was employed for modeling of ED. It was used to transform input data (concentration, temperature, flow rate and voltage) into a desired response (SP). With the aid of hidden layers, it can approximate virtually any input–output map. The well trained neural network can be used for prediction purpose. Fig. 5 illustrates the structure of the ANN used for modeling of ED.

5. Results and discussion

5.1. ANN model

Five important aspects that must be determined in design procedure of ANN are as follows:

- Data distribution in three subsets (training, validation and testing).
- Selection of neurons' transfer functions.
- Selection of ANN structure.
- Selection of training algorithm and its parameters.
- Selection of initial weights.
- Testing the ANN generalization.

5.1.1. Training, validation and testing data

As mentioned, MLP feed forward model was used in this study. The total 81 experimental data were randomly divided into three subsets of training, validation and testing for developing ANN model. Distribution of these data is shown in Fig. 6. Fifty training data were used to update the network weights and biases. In order to check the generality of network prediction and to prevent the data overfitting 21, validation data were applied. In the first few epochs of training, errors of both training and validation data are reduced. After several epochs, the error of training data decreases while that of validation data increases. As a result, the network is overtrained and its generality decreases. Hence, the training process must be continued until the validation data error decreases. Testing data set is used to test the generality of trained network via unseen patterns (experimental data which are not used in training procedure). The network generalizes well when it sensibly interpolates these new patterns. Termination of training procedure at a proper time, i.e. when the minimum validation error is achieved, results in a generalized predictor network.

5.1.2. Training algorithm and transfer function

The MLP networks were created in the neural network toolbox of Matlab with *newff* function. Performances of different training algorithms were studied for a specified network with four layers (1 input layer/2 hidden layer/1 output layer). Due to the convergence speed and the performance of network to find better solution, the Levenberg–Marquardt training method was selected as a proper training algorithm in agreement with the literature [23,24,29,46,47,52,64].

Another important factor in ANN design is the type of transfer functions. ANNs owe their nonlinear capability to the use of nonlinear transfer functions [48]. Different transfer functions can be used for neurons in the different layers. Different transfer functions were examined in each layer, separately and with respect to the mean squared error (MSE) of testing data, the proper transfer functions were chosen. MSE is calculated as follows:

$$\mathrm{MSE} = \frac{\sum_N (\mathrm{SP_{cal}} - \mathrm{SP_{exp}})^2}{N} \quad (19)$$

where subscripts cal and exp denote calculated and experimental values of SP, respectively. N is the number of validation and training data.

The most widely used criteria including MSE, root mean square error (RMSE), correlation coefficient (R), coefficient of determination (R^2) and mean squared relative error (MSRE) for training, validation and testing data sets are presented in Table 3. RMSE is the square root of MSE presented in Eq. (19). In probability theory and statistics, R indicates the strength and direction of a linear relationship between two variables. In general statistical usage, R refers to the departure of two variables from independence. A number of different coefficients are used for different situations. The best known is the Pearson product-moment correlation coefficient as follows:

$$R = \frac{\sum_N (\mathrm{SP_{cal}} - \mathrm{SP_{cal,ave}})(\mathrm{SP_{exp}} - \mathrm{SP_{exp,ave}})}{\sqrt{\sum_N (\mathrm{SP_{cal}} - \mathrm{SP_{cal,ave}})}\sqrt{\sum_N (\mathrm{SP_{exp}} - \mathrm{SP_{exp,ave}})}}$$

R^2 can have only positive values ranging from $R^2 = +1.0$ for a perfect correlation (positive or negative) down to $R^2 = 0.0$ for a complete absence of correlation. The advantage of R is that it provides the positive or negative direction of the correlation. The advantage of R^2 is that it provides a measure of the strength of the correlation. It can be said that R^2 represents the proportion of the data that is the closest to the line of best fit.

Table 3
Statistical criteria for evaluation of ANN model

Criterion	Training data	Validation data	Testing data	Total ANN
MSE	0.019	0.260	0.444	0.102
RMSE	0.137	0.509	0.666	0.319
R	0.999	0.999	0.999	0.999
R^2	0.999	0.998	0.998	0.999
MSRE	0.004	0.001	0.011	0.004

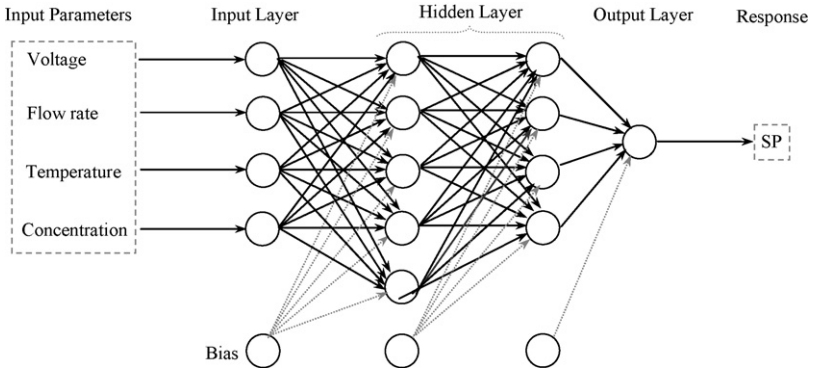

Fig. 5. Structure of a typical ANN used for modeling of ED.

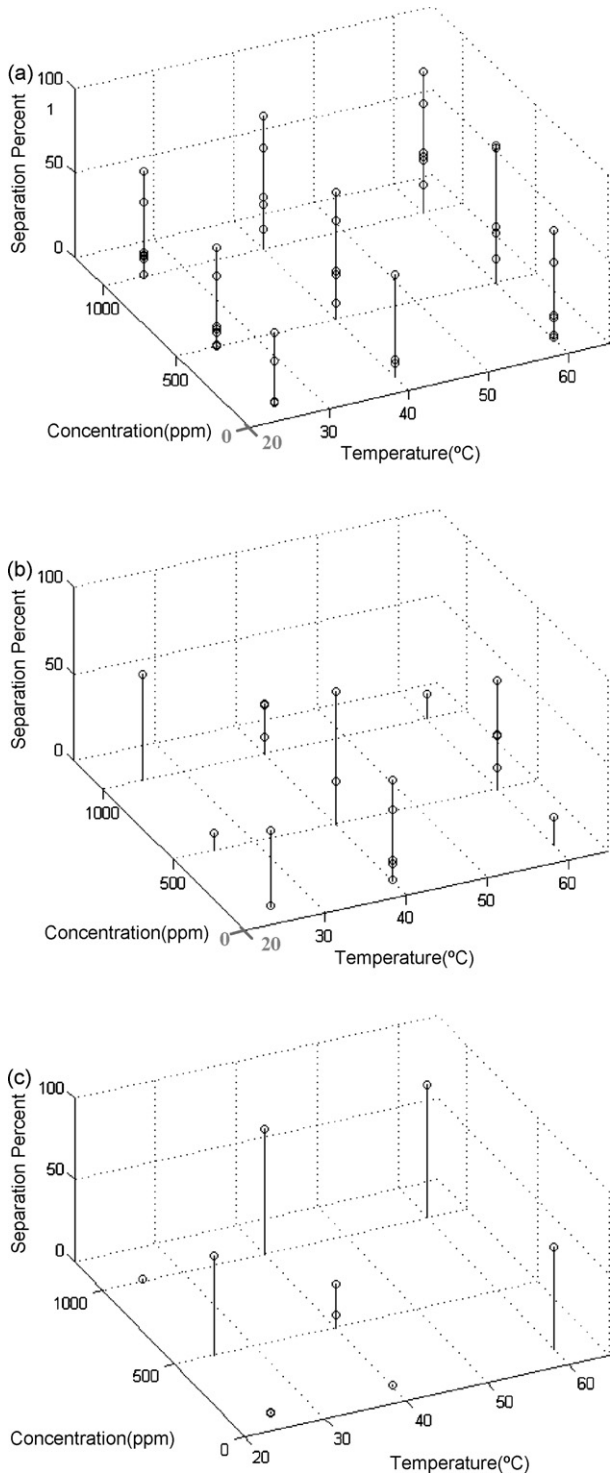

Fig. 6. Distribution of (a) training, (b) validation and (c) testing data subsets.

Another measure of fit is MSRE which is calculated by the following equation:

$$\mathrm{MSRE} = \frac{1}{N}\sum_{N}\left(\frac{\mathrm{SP_{cal}} - \mathrm{SP_{exp}}}{\mathrm{SP_{exp}}}\right)^2 \quad (20)$$

According to data presented in Table 3, excellent fitness of ANN predicted values with experimental data was confirmed.

Among different transfer functions available in Matlab, log sigmoid function was selected for all neurons due to its better prediction performance than other transfer functions. The log sigmoid function is bounded between 0 and 1, so the input and output data should be normalized to the same range as the transfer function used. In other words, the logarithmic sigmoid transfer function gives scaled outputs (SP) in this range (0–1).

5.1.3. ANN structure

Network structure has significant effects on the predicted results. The number of input and output nodes, as mentioned before, is equivalent to the number of input and output data, respectively (4 and 1 in this work). However, the optimal number of hidden layers and the optimal number of nodes in each layer, are case dependent and there is no straightforward method for determination of them. Hornik showed that MLP feed forward networks with one hidden layer and sufficiently large neurons can map any input to each output to an arbitrary degree of accuracy [73]. However, Flood and Kartam reported that many functions are difficult to approximate well with one hidden layer [74]. They revealed that use of more than one hidden layer provides greater flexibility and enables the approximation of complex functions with fewer neurons. Baughman and Liu found out that adding a second hidden layer improves the network prediction capability significantly without having any detrimental effects on the generalization of the testing data set [64]. However, adding a third hidden layer results in a prediction capability similar to that of two hidden layer network, but it requires longer training times due to its more complex structure.

In this study, structures including 1–10 neurons in the first hidden layer and 1–10 neurons in the second hidden layer as well as structures with single hidden layer of 1–10 neurons were investigated. Among them 4:5:4:1 network (2 hidden layers with 5 and 4 neurons in the first and second layer, respectively), as illustrated in Fig. 5, showed the minimum MSE, R and MSRE for validation data set (0.260, 0.999 and 0.001, respectively) and therefore has been selected as the proper structure.

Another important factor that affects the performance of networks is selection of the initial weights. In this work, Nguyen–Widrow algorithm was used to initialize the weights of layers and biases. This algorithm chooses values in order to distribute the active region of each neuron in the layer approximately

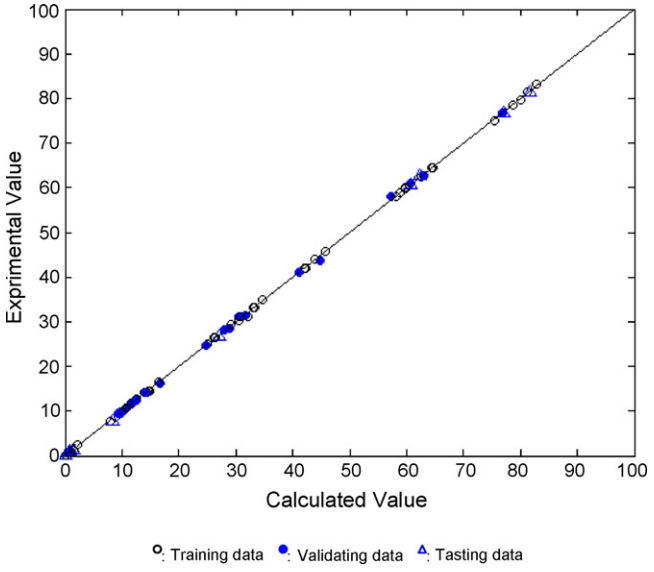

Fig. 7. Performance of 4:5:4:1 network at the minimum MSE of validation data.

evenly across the layer's input space [63]. The wrong choice of initial weights can lead to the local minimum values and therefore bad performance of the networks. In order to prevent these phenomena, 20 runs were performed using different random values of initial weights and the best trained network was selected.

In Fig. 7, the experimental results versus neural network predictions of the selected network (4:5:4:1) is plotted at the minimum MSE of validation data. According to this figure, excellent performance of the 4:5:4:1 network is confirmed.

5.1.4. ANN generalization

The selected network was used to predict SP for different inputs in the domain of training data. In Fig. 8, SP is plotted versus operating parameters in 3D plots. As can be seen, the generalization performances of 4:5:4:1 network, show no oscillations and this confirms an excellent prediction performance of ANN. ANN predictions can also be used for optimization purposes.

5.2. MM

In order to assess the reliability of MM, the calculated results were compared with the measured experimental data. MM prediction values and experimental data are depicted in Fig. 9. As can be seen in Fig. 9a, at low and medium voltages ($10 < V < 20$) and all flow rates, MM offers reasonable results.

According to Fig. 9b, it is found that there is an acceptable agreement between the calculated results and experimental data

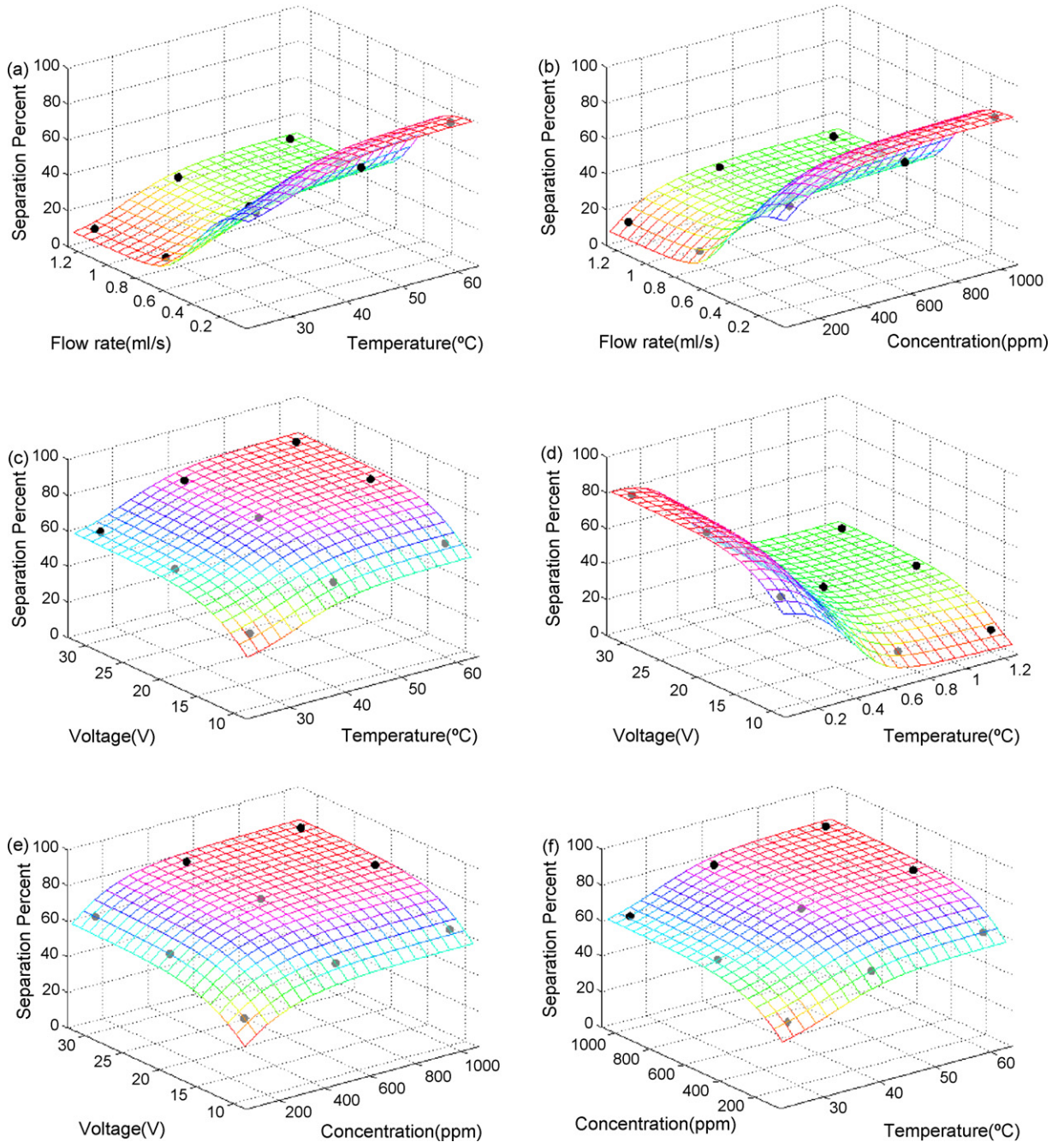

Fig. 8. Generalization performances of optimal ANN, effects of (a) flow rate and temperature at 500 ppm and 30 V, (b) flow rate and concentration at 30 V and 60 °C, (c) voltage and temperature at 500 ppm and 0.07 mL/s, (d) voltage and flow rate at 500 ppm and 60 °C, (e) voltage and concentration at 0.07 mL/s and 60 °C and (f) concentration and temperature at 0.07 mL/s and 30 V on SP.

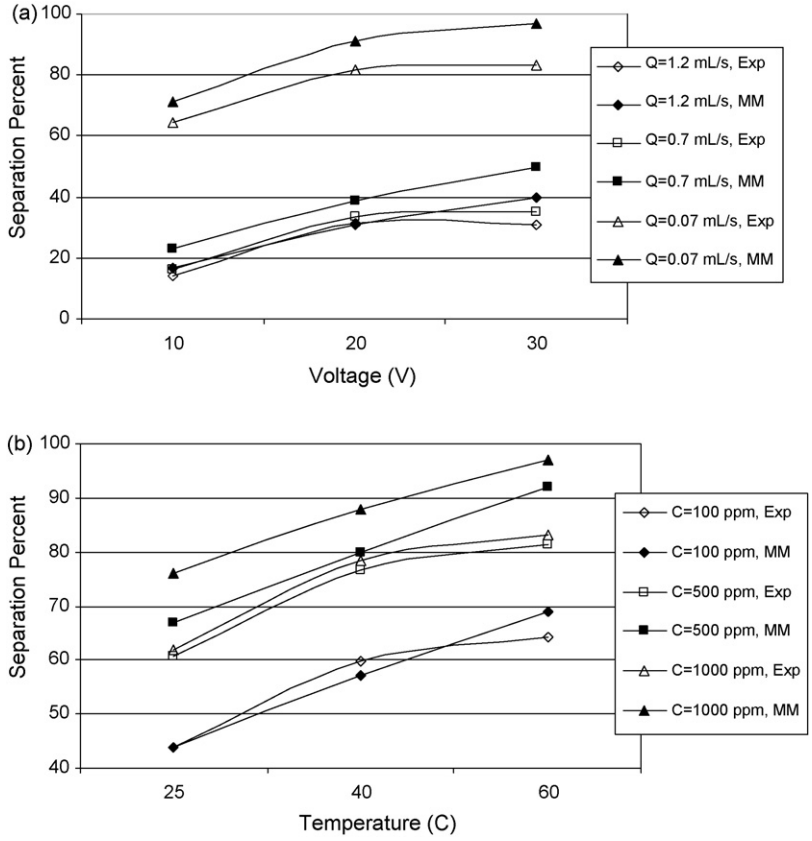

Fig. 9. MM prediction values compared with experimental data, (a) effect of voltage on SP at different flow rates and (b) effect of temperature on SP at different feed concentration, both plotted at optimum levels of two other factors, i.e. $C = 1000$ ppm, $T = 60\,^{\circ}C$, $Q = 0.07$ mL/s and $V = 30$ V.

at lower temperatures and concentrations ($100\text{ ppm} < C < 500\text{ ppm}$ and $25\,^{\circ}C < T < 40\,^{\circ}C$).

It should be noted that, although experimental values and MM curves do not completely coincide with each other (significant deviations are observed in some cases), they properly describe the trend of the behavior. Obviously, it can be said that MM is of great importance because (1) it satisfies experimental data to a moderately sufficient degree of correlation coefficient (0.97), (2) it can be used for different scale of ED cells and ions, (3) it can be easily used to calculate SP at

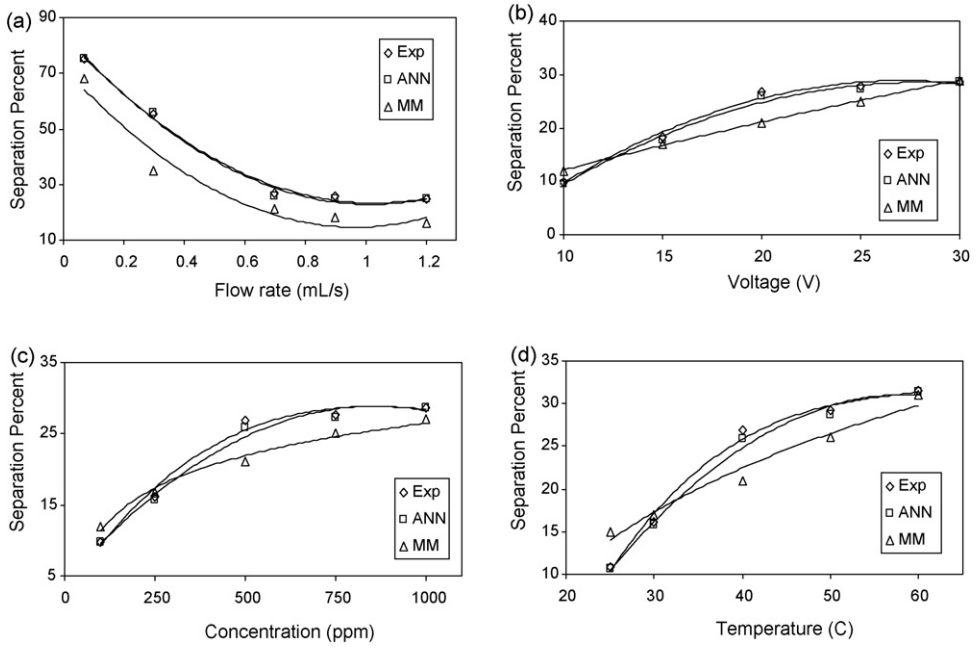

Fig. 10. Comparing MM, ANN and experimental data, effect of (a) flow rate, (b) voltage, (c) concentration and (d) temperature on SP at medium levels of other factors, i.e. $C = 500$ ppm, $T = 40\,^{\circ}C$, $Q = 0.7$ mL/s and $V = 20$ V.

Table 4
Comparing of the performance of MM and ANN model

Criterion	MM	ANN
MSE	38.605	0.102
RMSE	6.213	0.319
R	0.975	0.999
R^2	0.950	0.999
MSRE	23.949	0.004

different operational conditions, (4) it can be used for scale up.

5.3. Comparing MM and ANN

MM, ANN modeling predictions and experimental data were juxtaposed in Fig. 10. As can be seen, ANN can predict SP of ED cell at various operating conditions much better than MM. Better performance of ANN model was confirmed by comparing MSE, RMSE, R, R^2 and MSRE of two models in Table 4.

Excellent agreement between ANN results and experimental data indicates the capability of ANN to model the complicated ion transfer mechanism in an electrical field. Fig. 10b–d confirms that MM tends to describe the nonlinear behavior of ED process in almost a linear manner.

According to Fig. 10, increasing voltage, concentration and temperature increase SP values. It is obvious due to the fact that increasing temperature and concentration decreases the solution resistance, while increasing voltage increases the driving force. At higher flow rates, SP values decrease because the more flow rate means the less residence time, and thus, ions that are between the membranes do not have enough time to transfer through them.

Taking a closer look to Fig. 10, it is found that the differences between SP values regarding medium and high levels of parameters are negligible comparing to those regarding low and medium levels. i.e., at higher values of parameters, almost constant values of SP are achieved.

6. Conclusion

MM and ANN modeling were employed for prediction of ED; a wastewater treatment process. A multilayer network (FFNN–MLP), with two hidden layers (4:5:4:1), was applied to predict SP of Pb^{2+} ions in the dilute compartment of a laboratory scale ED cell. The MM was derived using an ED channel mass balance and its parameter was calculated using the experimental data of lead ions.

ANN successfully tracked the nonlinear behavior of SP versus temperature, voltage, concentration and flow rate with MSE, R and MSRE of 0.102, 0.999 and 0.004, respectively.

The developed MM makes it possible to predict SP of an ED cell at different operating conditions and ions as well as different cell dimensions. It means that the MM expresses the actual behavior of an ED system in spite of great deviations from experimental data observed in some cases (MSE, R and MSRE of 38.605, 0.975 and 23.949).

ANN modeling technique was found out to have many favorable features such as efficiency, generalization and simplicity, which make it an attractive choice for modeling of complex systems, such as wastewater treatment processes.

References

[1] P. Canizares, A. Perez, R. Camarillo, Recovery of heavy metals by means of ultrafiltration with water-soluble polymers: calculation of design parameters, Desalination 144 (2002) 279–285.
[2] T. Mohammadi, A. Razmi, M. Sadrzadeh, Effect of operating parameters on Pb^{2+} separation from wastewater using electrodialysis, Desalination 167 (2004) 379–385.
[3] P. Zhou, J.C. Huang, A.W.F. Li, S. Wei, Heavy metal removal from wastewater in fluidized bed reactor, Water Res. 33 (1999) 1918–1924.
[4] S.R. E1-Hasani, S.M. AI-Dhaheri, M.S. El-Maazawi, M.M. Kamal, Polarographic and voltammetric determination of some toxic heavy metal ions in the treated wastewater at Abu-Dhabi, UAE, Water Sci. Technol. 40 (1999) 67–74.
[5] E. Rodryguez de San Miguel, J.C. Aguilar, M.T.J. Rodryguez, J. De Gyves, Solvent extraction of Ga (III), Cd (II), Fe (III), Zn (II), Cu (II), and Pb (II) with ADOGEN 364 dissolved in kerosene from 1 to 4 tool dmy3 HCI media, Hydrometallurgy 57 (2000) 151–165.
[6] A.R.K. Dapaah, N. Takano, A. Ayame, Solvent extraction of Pb(II) from acid medium with zinc hexamamethylenedithiocarbamate followed by backextraction and subsequent determination by FAAS, Anal. Chim. Acta 386 (1999) 281–286.
[7] V.J. Inglezakis, M.D. Loizidou, H.P. Grgorooulou, Equilibrium and kinetic ion exchange studies of Pb^{2+}, Cr^{3+}, Fe^{3+} and Cu^{2+} on natural clinoptilolite, Water Res. 36 (2002) 2784–2792.
[8] M.V. Mier, R.L.P. Callejas, R. Gehr, B.E.J. Cisneros, P.J.J. Alvarez, Heavy metal removal with Mexican clinoptilolite: multi-component ionic exchange, Water Res. 35 (2001) 373–378.
[9] A. Vecchio, C. Finoli, D. Di Simine, V. Andreoni, Heavy metal biosorption by bacterial cells, Fresenius J. Anal. Chem. 361 (1998) 338–342.
[10] M.L. Merroun, N. Ben Omar, M.T. Gonzalez Munoz, J.M. Arias, Removal of lead from aqueous solutions by *Myxococcus xanthus*, Int. Biodet. Biodeg. 37 (1996) 241.
[11] M. Bustard, A.P. McHale, Biosorption of heavy metals by distillery-derived biomass, Bioprocess Eng. 19 (5) (1998) 351–353.
[12] A.A. Pradhan, A.D. Levine, Microbial biosorption of copper and lead from aqueous systems, Sci. Total Environ. 170 (1995) 209–220.
[13] J.M. Brady, J.M. Tobin, Binding of hard and soft metal ions to *Rhizopus arrhizus biomass*, Enzyme Microbiol. Technol. 17 (1995) 791–796.
[14] V. Gopal, G.C. April, V.N. Schrodt, Selective lead ion recovery from multiple cation waste streams using the membrane-electrode process, Sep. Purif. Technol. 14 (1998) 85–93.
[15] K. Basta, A. Aliane, A. Lounis, R. Sandeaux, J. Sandeaux, C. Gavach, Electroextraction of Pb^{2+} ions from dilute solutions by a process combining ion-exchange textiles and membranes, Desalination 120 (1998) 175–184.
[16] R.S. Juang, S.W. Wang, Metal recovery and EDTA recycling from simulated washing effluents of metal contaminated soils, Water Res. 34 (2001) 3795–3803.
[17] G. Banerjee, S. Sarker, The role of salvinia rotundifolia in scavenging aquatic Pb(II) pollution: a case study, Bioprocess Eng. 17 (1997) 295–300.
[18] W.S. Winston Ho, K.K. Sirkar, Membrane Handbook, Champan & Hall, 1992.
[19] T. Mohammadi, A. Kaviani, Water shortage and seawater desalination by electrodialysis, Desalination 158 (2003) 267–270.
[20] T. Mohammadi, A. Moheb, M. Sadrzadeh, A. Razmi, Separation of copper ions by electrodialysis using Taguchi experimental design, Desalination 169 (2004) 21–31.
[21] W. Sha, K.L. Edwards, The use of artificial neural networks in materials science based research, Mater. Des. 28 (2007) 1747–1752.
[22] F.S. Mjalli, S. Al-Asheh, H.E. Alfadala, Use of artificial neural network black-box modeling for the prediction of wastewater treatment plants performance, J. Environ. Manage. 83 (2007) 329–338.
[23] G.B. Sahoo, C. Ray, Predicting flux decline in cross-flow membranes using artificial neural networks and genetic algorithms, J. Membr. Sci. 283 (2006) 147–157.
[24] H. Chen, A.S. Kim, Prediction of permeate flux decline in cross-flow membrane filtration of colloidal suspension: a radial basis function neural network approach, Desalination 192 (2006) 415–428.
[25] M. Dornier, M. Decloux, G. Trystram, A. Lebert, Dynamic modeling of crossflow microfiltration using neural networks, J. Membr. Sci. 98 (1995) 263–273.
[26] E. Piron, E. Latrille, F. Rene, Application of artificial neural networks for crossflow microfiltration modelling: "black-box" and semiphysical approaches, Comput. Chem. Eng. 21 (9) (1997) 1021–1030.
[27] M. Hamachi, M. Cabassud, A. Davin, M.M. Peuchot, Dynamic modeling of crossflow microfiltration of bentonite suspension using recurrent neural networks, Chem. Eng. Process. 38 (1999) 203–210.
[28] C. Aydiner, I. Demir, E. Yildiz, Modeling of flux decline in crossflow microfiltration using neural networks: the case of phosphate removal, J. Membr. Sci. 248 (2005) 53–62.
[29] S. Chellam, Artificial neural network model for transient crossflow microfiltration of polydispersed suspensions, J. Membr. Sci. 1/2 (2005) 35–42.
[30] N. Delgrange, C. Cabassud, M. Cabassud, L. Durand-Bourli, J.M. Laine, Modeling of ultrafiltration fouling by neural network, Desalination 118 (1998) 213–227.
[31] N. Delgrange, C. Cabassud, M. Cabassud, L. Durand-Bourli, J.M. Laine, Neural networks for prediction of ultrafiltration transmembrane pressure – application to drinking water production, J. Membr. Sci. 150 (1998) 111–123.
[32] W.R. Bowen, M.G. Jones, H.N.S. Yousef, Dynamic ultrafiltration of proteins-a neural network approach, J. Membr. Sci. 146 (1998) 225–235.
[33] W.R. Bowen, M.G. Jones, H.N.S. Yousef, Prediction of the rate of crossflow membrane ultrafiltration of colloids: a neural network approach, Chem. Eng. Sci. 53 (22) (1998) 3793–3802.
[34] C. Teodosiu, O. Pastravanu, M. Macoveanu, Neural network models for ultrafiltration and backwashing, Water Res. 34 (2000) 4371–4380.
[35] N. Delgrange-Vincent, C. Cabassud, M. Cabassud, L. Durand- Bourlier, J.M. Laine, Neural networks for long term prediction of fouling and backwash efficiency in ultrafiltration for drinking water production, Desalination 131 (2000) 353–362.

[36] W.R. Bowen, H.N.S. Yousef, J.I. Calvo, Dynamic crossflow ultrafiltration of colloids: a deposition probability cake filtration approach, Sep. Purif. Technol. 24 (2001) 297–308.
[37] C. Bhattacharjee, M. Singh, Studies on the applicability of artificial neural network (ANN) in continuous stirred ultrafiltration, Chem. Eng. Technol. 25 (12) (2002) 1187–1192.
[38] M. Cabassud, N. Delgrange-Vincent, C. Cabassud, L. Durand- Bourlier, J.M. Laine, Neural networks: a tool to improve UF plant productivity, Desalination 145 (2002) 223–231.
[39] S. Curcio, V. Calabro, G. Iorio, Monitoring and control of TMP and feed flow rate pulsatile operations during ultrafiltration in a membrane module, Desalination 145 (1–3) (2002) 217–222.
[40] S.M.A. Razavi, S.M. Mousavi, S.A. Mortazavi, Dynamic prediction of milk ultrafiltration performance: a neural network approach, Chem. Eng. Sci. 58 (2003) 4185–4195.
[41] S.M.A. Razavi, S.M. Mousavi, S.A. Mortazavi, Dynamic modeling of milk ultrafiltration by artificial neural network, J. Membr. Sci. 220 (18) (2003) 47–58.
[42] S. Curcio, V. Calabro, G. Iorio, Integration of Matlab and LabWiew to design innovative control systems applicable to membrane processes, in: Proceedings of the EuroMembrane 2004, Hamburg, Germany, September 28–October 01, 2004.
[43] P. Rai, G.C. Majumdar, S. DasGupta, S. De, Modeling the performance of batch ultrafiltration of synthetic fruit juice and mosambi juice using artificial neural network, J. Food Eng. 71 (2005) 273–281.
[44] S. Curcio, G. Scilingo, V. Calabro, G. Iorio, Ultrafiltration of BSA in pulsating conditions: an artificial neural networks approach, J. Membr. Sci. 246 (2) (2005) 235–247.
[45] S. Curcio, V. Calabro, G. Iorio, Reduction and control of flux decline in crossflow membrane processes modeled by artificial neural networks, J. Membr. Sci. 286 (2006) 125–132.
[46] G.R. Shetty, S. Chellam, Predicting membrane fouling during municipal drinking water nanofiltration using artificial neural Networks, J. Membr. Sci. 217 (2003) 69–86.
[47] G.R. Shetty, H. Malki, S. Chellam, Predicting contaminant removal during municipal drinking water nanofiltration using artificial neural networks, J. Membr. Sci. 212 (2003) 99–112.
[48] W.R. Bowen, M.G. Jones, J.S. Webfoot, H.N.S. Yousef, Predicting salt rejection at nanofiltration membranes using artificial neural networks, Desalination 129 (2000) 147–162.
[49] H. Al-Zoubi, N. Hilal, N.A. Darwish, A.W. Mohammad, Rejection and modeling of sulphate and potassium salts by nanofiltration membranes: neural network and Spiegler–Kedem model, Desalination 206 (2007) 42–60.
[50] H. Niemi, A. Bulsari, S. Palosaari, Simulation of membrane separation by neural networks, J. Membr. Sci. 102 (1995) 185–191.
[51] Y. Zhao, J.S. Taylor, S. Chellam, Predicting RO/NF water quality by modified solution diffusion model and artificial neural networks, J. Membr. Sci. 263 (2005) 38–46.
[52] A. Abbas, N. Al-Bastaki, Modeling of an RO water desalination unit using neural networks, Chem. Eng. J. 114 (2005) 139–143.
[53] K. Al-Shayji, Y.A. Liu, Neural networks for predictive modeling and optimization of large-scale commercial water desalination plants, Proc. IDA World Congress Desalination Water Sci. 1 (1997) 1–15.
[54] K. Al-Shayji, Y.A. Liu, Predictive modeling of large-scale commercial water desalination plants: data-based neural network and model-based process simulation, Ind. Eng. Chem. Res. 41 (25) (2002) 6460–6474.
[55] M.M. Jafar, A. Zilouchian, Adaptive receptive fields for radial basis functions, Desalination 135 (2001) 83–91.
[56] A. Shahsavand, M. Pourafshari Chenar, Neural networks modeling of hollow fiber membrane processes, J. Membr. Sci. 297 (2007) 59–73.
[57] L. Wang, C. Shao, H. Wang, H. Wu, Radial basis function neural networks based modeling of the membrane separation process: hydrogen recovery from refinery gases, J. Nat. Gas Chem. 15 (2006) 230–234.
[58] S. Geissler, T. Wintgens, T. Melin, K. Vossenkaul, C. Kullmann, Modeling approaches for filtration processes with novel submerged capillary modules in membrane bioreactors for wastewater treatment, Desalination 178 (2005) 125–134.
[59] O. Cinar, H. Hasar, C. Kinaci, Modeling of submerged membrane bioreactor treating cheese whey wastewater by artificial neural network, J. Biotechnol. 123 (2006) 204–209.
[60] W.Y. Lee, G.G. Park, T.H. Yang, Y.G. Yoon, C.S. Kim, Empirical modeling of polymer electrolyte membrane fuel cell performance using artificial neural networks, Int. J. Hydrogen Energy 29 (2004) 961–966.
[61] S. Ou, L.E.K. Achenie, A hybrid neural network model for PEM fuel cells, J. Power Sources 140 (2) (2005) 319–330.
[62] K.A. Al-Shayji, Modeling, simulation and optimization of large-scale commercial desalination plant, PhD thesis, Virginia Polytechnic Institute and State University, Virginia, USA, 1998.
[63] H. Demuth, M. Beale, Neural Network Toolbox: for use with MATLAB (Version 4.0), The Math Works, Inc., 2004.
[64] D.R. Baughman, Y.A. Liu, Neural Network in Bioprocessing and Chemical Engineering, Academic Press, San Diego, California, USA, 1995.
[65] J.A. Freeman, D.M. Skapura, Neural Networks Algorithms, Applications, and Programming Techniques, Addison-Wesley, Reading, Massachusetts, USA, 1992.
[66] S. Haykin, Neural Networks: A Comprehensive Foundation, Macmillan College Co., New York, USA, 1994.
[67] P. Mehra, B.W. Wah, Artificial Neural Networks: Concepts and Theories, IEEE Press, Los Alamitos, California, USA, 1992.
[68] M. Demircioglu, N. Kabay, Cost Comparison and Efficiency Modeling in the Electrodialysis of Brine, Desalination 136 (2001) 317–323.
[69] A.A. Sonin, M.S. Isaacson, Optimization of flow design in forced flow electrochemical systems, with special application to electrodialysis, Ind. Eng. Chem. Process Des. Dev. 13 (1974) 241–248.
[70] T. Mohammadi, A. Moheb, M. Sadrzadeh, A. Razmi, Modeling of metal ion removal from wastewater by electrodialysis, Sep. Purif. Technol. 41 (2005) 73–82.
[71] M. Sadrzadeh, A. Kaviani, T. Mohammadi, Mathematical modeling of desalination by electrodialysis, Desalination 206 (2007) 538–546.
[72] M. Sadrzadeh, A. Razmi, T. Mohammadi, Separation of different ions from wastewater at various operating conditions using electrodialysis, Sep. Purif. Technol. 54 (2007) 147–156.
[73] K. Hornik, M. Stinchombe, H. White, Multi-layer feedforward networks are universal approximations, Neural Networks 2 (1989) 359–366.
[74] I. Flood, N. Kartam, Neural networks in civil engineering. I. Principles and understanding, J. Comput. Civil Eng. 8 (1994) 131–148.